JAST (Journal of Animal Science and Technology) TITLE PAGE

ARTICLE INFORMATION	Fill in information in each box below
Article Type	Research article
Article Title (within 20 words without abbreviations)	A multi-omics characterization of the gut microbiota of weaned piglets in response to *Lactobacillus plantarum* supplementation
Running Title (within 10 words)	Multi-omics Analysis of Gut Microbiota in Weaned Piglets
Author	Nae-Ho Park1,†, Byeonghwi Lim1,2,†, Chiwoong Lim1, Young-Jun Seo1, Ji-Yeong Lee1,Jungwoo Yang3, Minjee Lee4, Kyeong Il Park5 ,Hyunjin Kyoung5, Minho Song5,*, and Jun-Mo Kim1,*
Affiliation	1 Department of Animal Science and Technology, Chung-Ang University, Anseong, Gyeonggi-do 17546, Republic of Korea 2 Department of Animal Science, Iowa State University, Ames, IA 50011, USA 3 Department of Microbiology, College of Medicine, Dongguk University, Gyeongju 38066, Republic of Korea 4 IBS R&D Center, Ildong Bioscience. Pyeongtaek 17957, Korea 5 Department of Animal Science and Biotechnology, Chungnam National University, Daejeon 34134, Republic of Korea
ORCID (for more information, please visit https://orcid.org)	Nae-Ho Park(https://orcid.org/0000-0002-3719-9004) Byeonghwi Lim (https://orcid.org/0000-0001-8489-0044) Chiwoong Lim (https://orcid.org/0000-0002-6272-4464) Young-Jun Seo (https://orcid.org/0000-0001-7520-7733) Ji-Yeong Lee (https://orcid.org/0000-0002-0775-7191) Jungwoo Yang (https://orcid.org/0000-0003-3836-729X) Minjee Lee (https://orcid.org/0000-0002-0594-5279) Kyeong Il Park (https://orcid.org/0000-0002-3590-3993) Hyunjin Kyoung (https://orcid.org/0000-0001-5742-5374) Minho Song (https://orcid.org/0000-0002-4515-5212) Jun-Mo Kim (https://orcid.org/0000-0002-6934-398X)
Competing interests	The authors declare no potential conflict of interest.
Funding sources State funding sources (grants, funding sources, equipment, and supplies). Include name and number of grant if available.	This work was supported by Korea Institute of Planning and Evaluation for Technology in Food, Agriculture and Forestry(IPET) through Agricultural Microbiome R&D Program for Advancing innovative technology Program(or Project), funded by Ministry of Agriculture, Food and Rural Affairs(MAFRA)(RS-2025-02216704) and was supported by the Chung-Ang University Research Grants in 2024.
Acknowledgements	Not applicable.
Availability of data and material	Upon reasonable request, the datasets of this study can be available from the corresponding author.
Authors' contributions Please specify the authors' role using this form.	Conceptualization: Park NH, Kim JM Data curation: Park NH, Lee M Formal analysis: Park NH, Yang J Methodology: Park NH, Lim B, Lim C, Lee JY Software: Seo YJ, Lee JY, Park KI, Kyoung H Validation: Seo YJ, Yang J, Lee M, Song M, Kim JM

	Investigation: Park NH, Song M Writing - original draft: Park NH Writing - review & editing: Park NH, Lim B, Lim C, Seo YJ, Lee JY, Yang J, Lee M, Kyoung H, Song M, Kim JM
Ethics approval and consent to participate	All animal experiments followed standard protocols and guidelines and received approval from the Institutional Animal Care and Use Committee of Chungnam National University, Daejeon, South Korea (approval # 202103A-CNU-079).

1

2 **CORRESPONDING AUTHOR CONTACT INFORMATION**

For the corresponding author (responsible for correspondence, proofreading, and reprints)	**Fill in information in each box below**
First name, middle initial, last name	Jun-Mo Kim
Email address – this is where your proofs will be sent	junmokim@cau.ac.kr
Secondary Email address	
Address	Department of Animal Science and Technology, Chung-Ang University, Anseong, Gyeonggi-do 17546, Republic of Korea
Cell phone number	+82-10-4026-5644
Office phone number	+82-31-670-3263
Fax number	+82-31-675-3108

3

For the corresponding author (responsible for correspondence, proofreading, and reprints)	**Fill in information in each box below**
First name, middle initial, last name	Minho Song
Email address – this is where your proofs will be sent	junmokim@cau.ac.kr
Secondary Email address	
Address	Department of Animal Science and Biotechnology, Chungnam National University, Daejeon 34134, Korea
Cell phone number	+82-10-9254-0931
Office phone number	+82-42-821-7857
Fax number	

4

ABSTRACT

Weaning is a critical developmental stage in piglets and is frequently associated with intestinal dysfunction, diarrhea, and growth retardation due to abrupt dietary and environmental changes. Probiotics have been explored as antibiotic alternatives to alleviate postweaning stress, and *Lactobacillus plantarum* has shown potential for modulating the gut microbiota and improving intestinal health. However, most previous studies have relied on single-omics approaches, limiting mechanistic understanding of host–microbiome interactions.

This study employed an integrated multi-omics approach combining ileal transcriptomics, fecal microbiomics, and metabolomics to investigate the effects of dietary *L. plantarum* supplementation in weaned piglets. Six piglets were assigned to either a control or *L. plantarum*-supplemented group for two weeks. RNA sequencing, 16S rRNA gene sequencing, and gas chromatography mass spectrometry based metabolomics were conducted, followed by integrative analysis using MIMOSA2 and MetaboAnalyst.

Transcriptomic analysis identified 1,229 differentially expressed genes enriched in immune-related pathways, including NF-κB and IgA signaling, as well as epithelial barrier regulation. Microbiome profiling revealed increased microbial diversity, enrichment of *Lactobacillus*, and reduced abundance of *Shigella*. Functional prediction suggested enhanced innate immune responsiveness. Integrated metabolome–transcriptome analysis highlighted lipid and amino acid metabolic pathways linking microbial metabolites with host gene expression.

Overall, *L. plantarum* supplementation induced coordinated host–microbiome

adaptations associated with reduced oxidative stress, improved intestinal barrier stability, and enhanced immune resilience. These findings provide mechanistic evidence supporting *L. plantarum* as a promising nutritional strategy to mitigate postweaning stress and improve piglet intestinal health.

Keywords:

Piglet, Microbiota, Multi-Omics Integration, *Lactobacillus*, Gut

1. Introduction

Weaning is an important part of the pig lifecycle. During the weaning period, piglets encounter various environmental challenges such as separation from the sow, changes in diet, culminating in changes in the intestinal environment (1). This may induce diarrhea, which results in reduced growth rate and mortality in piglets (2). Reports from large-scale pig production systems indicate that post-weaning diarrhea can affect up to 50% of piglets, with mortality rates increasing to 15–20%, underscoring the considerable impact of weaning-related gastrointestinal challenges on herd health and farm profitability (3). To address these challenges, several studies have been conducted to alleviate weaning stress, reduce diarrhea, and enhance pig growth. Previous studies have shown that probiotic feed additives can improve nutrient utilization, feed efficiency, and growth-related performance in pigs by supporting intestinal function (4). In particular, L. plantarum-based feed additives may support postweaning productivity by improving intestinal morphology and nutrient absorption (5), as well as resilience against diarrhea-associated growth retardation through pathogen suppression and host defense modulation (6). These effects are closely associated with intestinal environmental changes, including increased villus height, modulation of gut microbiota, suppression of opportunistic pathogens, and stimulation of local immune responses (5, 6).

Antibiotics have traditionally been used to control diseases in livestock. However, their continuous application disrupts the gut microbiota and accelerates the spread of antimicrobial resistance, raising significant public health concerns (7, 8). To address these challenges, probiotics have emerged as promising alternatives to promote

swine health and performance. Probiotics, including *Lactobacillus plantarum*, help maintain balanced intestinal microbiota, suppress opportunistic pathogen growth, and stimulate local immune responses (4, 6). Recent studies have reported that *L. plantarum* supplementation is associated with increased villus height in the ileum, jejunum, and duodenum, thereby enhancing nutrient absorption and strengthening the gut barrier against pathogens (5). Collectively, probiotics contribute to the stabilization of intestinal function and resilience, ultimately supporting animal growth and productivity.

Previous studies have investigated the effects of *L. plantarum* on weaned piglets; however, most have relied on a single-omics approach (5, 9). Although studies provide valuable insights, the complexity and interconnectedness of biological systems in animals make it difficult to fully capture host responses through single-omics analysis alone. To overcome these limitations, this study employed an integrated multi-omics approach, combining transcriptomics, metabolomics, and microbiomics data. This systematic integration enables a more comprehensive characterization of the interplay between gene expression patterns, metabolic alterations, and microbial community dynamics, thereby offering deeper insights into the mechanisms by which *L. plantarum* influences piglet development and health.

The ileum, which is the terminal segment of the small intestine, is structurally characterized by abundant villi and microvilli that expand its absorptive surface. In addition to its role in nutrient absorption, the ileum contains Peyer's patches—specialized lymphoid structures—that function as key sites for initiating mucosal immune responses (10). Although the ileum does not directly secrete digestive enzymes, it depends on enzymes from the jejunum for complete digestion and nutrient

uptake. Given its dual roles in nutrient assimilation and mucosal immunity, the ileum is regarded as a critical region for intestinal health evaluation. Previous studies have shown that probiotics, particularly *L. plantarum*, can influence ileal physiology by enhancing the villus architecture and modulating immune activity, thereby contributing to intestinal barrier integrity and overall gut function (5).

In this study, we aimed to elucidate the biological mechanisms underlying host–microbiome interactions mediated by intestinal metabolites in weaned piglets and identify key molecular pathways and microbial signatures that contribute to gut health and development during the critical weaning transition. Using an integrated multi-omics framework, specifically one that combines transcriptomics, metabolomics, and microbiological data, this study provides a comprehensive framework for understanding how *L. plantarum* shapes the intestinal ecosystems of weaned piglets. These insights may inform the development of targeted nutritional or microbial interventions to promote intestinal integrity, enhance immune function, and improve growth performance in swine production.

2. Methods

2.1 Animals and experimental design

Six piglets [(Landrace × Yorkshire) × Duroc] were weaned at 28 days of age and used in this study. The animals were randomly assigned to one of two treatment groups (n = 3 per group): a control group fed a standard corn–soybean meal-based diet, and a treatment group receiving the same basal diet supplemented with 0.02% *L. plantarum* IDCC 3501 (CON + *L. plantarum*), providing 2 × 10^9 CFU/g of probiotic. Each pig was housed individually in a pen (232 × 175 cm) equipped with a slatted plastic floor, feeder, and ad libitum access to water. The ambient temperature was maintained at 28–30°C, and relative humidity was controlled at 55 ± 5%, under a 12-h light/dark cycle. Diets were formulated to meet or exceed the nutritional requirements of the weaning pigs (NRC, 2012), and the ingredient and calculated nutrient compositions of the basal diet are provided in Supplementary Table S1. After a 2-week feeding period, ileal tissue and fecal samples were collected from three pigs per group. Ileal tissues were used for transcriptomic analysis via RNA sequencing, and fecal samples were subjected to 16S rRNA gene sequencing for microbiota profiling and untargeted metabolomic analysis using gas chromatography–mass spectrometry (GC–MS).

2.2 Sample collection

After the 2-week feeding period (day 14 post weaning), fecal samples were collected from all pigs (n = 3 per group) and immediately stored at –80 °C for downstream microbiome and metabolomic analyses. Following sample collection, the

pigs were euthanized and ileal tissue samples were obtained for transcriptomic analysis. Approximately 3 cm segments of the ileum were excised, gently rinsed with sterile saline, and immersed in RNAlater® solution (QIAGEN GmbH, Hilden, Germany) at room temperature for 24 h. The stabilized samples were then stored at –80 °C until RNA extraction.

2.3 Preparation of 16S rRNA Gene Amplicon Libraries

To characterize the fecal microbiota, the V3–V4 regions of the 16S rRNA gene were amplified using a standard Illumina 16S Metagenomic Sequencing Library Preparation protocol. Genomic DNA (2 ng per sample) was subjected to PCR in a reaction mixture containing 5 × reaction buffer, 1 mM dNTPs, 500 nM of each universal primer, and Herculase II Fusion DNA Polymerase (Agilent Technologies, Santa Clara, CA, USA). The thermal cycling conditions were as follows: initial denaturation at 95°C for 3 min; 25 cycles of 95°C for 30 s, 55°C for 30 s, and 72°C for 30 s; and a final extension at 72°C for 5 min. The primer pair used for the amplification included Illumina adapter overhang sequences: V3-F (5'-GTCGGCAGCGTCAGATGTGTATAAGAGACAGCCTACGGGNGGCWGCAG-3') and V4-R (5'-GTCTCGTGGGCTCGGAGATGTGTATAAGAGACAGGACTACHVGGGTATCTAATCC-3'). The initial amplicons were purified with AMPure beads (Agencourt Bioscience, Beverly, MA, USA). Two microliters of the purified product was then re-

amplified with Nextera XT index primers to incorporate dual indices and Illumina adapters. This indexing PCR was performed under the same thermal profile as the first reaction, but for only 10 cycles. The indexed products were purified again using AMPure beads, after which the library concentration was determined by quantitative PCR using the KAPA Library Quantification Kit for Illumina. Library size distribution and integrity were verified using the TapeStation system with a D1000 ScreenTape (Agilent Technologies, Waldbronn, Germany). Equimolar pooled libraries were sequenced using an Illumina MiSeq instrument (2 × 300 bp paired-end reads) at Macrogen, Inc.

2.4 Microbial community profiling and taxonomic classification

Cutadapt v3.7 (Marcel, 2011) was used to trim adapter sequences from raw 16S rRNA gene reads. All sequences were processed using QIIME2 version 2022.8. To correct sequencing errors and remove noise, amplicon sequence variants (ASVs) were inferred using the DADA2 algorithm (11). The ASVs were taxonomically assigned by aligning them to the SILVA v138_99 reference database with 99% similarity. The V3–V4 hypervariable regions of the 16S rRNA gene were annotated using a Naïve Bayes classifier trained with the q2-feature-classifier plugin.

To assess within-sample microbial diversity, alpha diversity was estimated using multiple indices, including the ACE, Chao1, Shannon, and Simpson indices, which provide complementary measures of species richness and evenness. These metrics were calculated using the QIIME2 core metrics phylogenetic pipeline, and statistical comparisons between groups were performed using the alpha group significance plugin.

Taxonomic classification was further refined by assigning ASVs to known taxonomic groups based on sequence similarity in the SILVA database, enabling detailed characterization of the microbial composition across treatment conditions.

2.5 RNA Sequencing and Data Processing

Total RNA was isolated from ileal tissue using TRIzol reagent (Invitrogen, Life Technologies, Carlsbad, CA, USA) following the manufacturer's protocol (12). The concentration and purity of the RNA were assessed using a NanoDrop ND-1000 spectrophotometer (NanoDrop Technologies, Wilmington, DE, USA). Library preparation was performed using 1 μg of total RNA with the Illumina TruSeq™ RNA Sample Preparation Kit. Paired-end sequencing (2 × 100 bp) was performed using an Illumina HiSeq 2000 platform (Illumina, San Diego, CA, USA). Detailed sequencing quality metrics for each sample are provided in Supplementary Table S2.

During library construction, messenger RNA was fragmented into short segments, which were then reverse-transcribed into first-strand cDNA using random primers and reverse transcriptase. Second-strand synthesis was performed using DNA Polymerase I and RNase H, followed by end repair and adapter ligation.

Quality control of raw reads was performed using FastQC v0.12.1 (13), and low-quality bases and adapter sequences were removed with Trimmomatic v0.39 (14), using the parameters SLIDINGWINDOW:4:15 and MINLEN:36. The cleaned reads were re-evaluated for quality using FastQC and aligned to the pig reference genome (Sus_scrofa.Sscrofa11.1.112) obtained from the Ensembl genome browser using HISAT2 v2.2.1, with the default settings (15).

Aligned reads were sorted and converted into BAM format using Samtools

v1.19.2 (16). Gene-level read counts were obtained using the featureCounts function in the Subread package (17), based on exon annotations from the Ensembl GTF file version 112.

Differential gene expression analysis was conducted using the edgeR package v3.40.2 in the bioconductor environment (18). Genes with fewer than 10 raw counts across all samples were excluded to ensure statistical robustness. Count data were normalized using the trimmed mean of M-values method (18). Multidimensional scaling analysis was performed using the limma package (19), and visualization was performed using the ggplot2 package (20) to assess sample clustering.

Differentially expressed genes (DEGs) were identified based on a false discovery rate (FDR) threshold of 0.05, adjusted using the Benjamini–Hochberg method, and a minimum absolute $\log_2$ fold change of 1.

2.6 Identification of DEGs and Functional Annotation

To investigate the biological significance of DEGs, functional enrichment analysis was performed using Gene Ontology (GO) biological processes (21) and Kyoto Encyclopedia of Genes and Genomes (KEGG) pathway annotations (22). Functional annotation and enrichment were performed using the Database for Annotation, Visualization, and Integrated Discovery (DAVID) v2022 (23).

GO terms were filtered using the "DIRECT" annotation option to ensure specificity, and enrichment analysis was conducted with the following thresholds: *P*-value < 1 and gene count ≥ 2 for initial filtering, followed by *P*-value < 0.1 and count ≥ 2 for significance. KEGG pathway enrichment analyses were performed using the same criteria. Enrichment results were reported as $-\log_{10}$(*P*-value) and fold enrichment

values for each pathway, with significance assessed directly from the enrichment test *P*-values rather than corrected *q*-values.

To improve interpretability, the enriched GO terms were grouped based on their semantic similarity using the REVIGO tool (24). Tree map visualizations were generated to highlight the representative GO terms from each functional group, emphasizing the most statistically significant terms in each cluster.

2.7 Metabolomic Sample Preparation and GC–MS Analysis

For untargeted metabolomic profiling, fecal samples were extracted using ice-cold 100% methanol at a ratio of 0.5 mL per 100 µL of sample volume. The extraction procedure consisted of three cycles of 1-min vigorous vortexing, interspersed at 1-min intervals on ice to enhance metabolite solubilization. Following extraction, samples were centrifuged at 16,000 × g for 5 min at 4°C, and the resulting supernatants were filtered using 0.2 µm polyvinylidene fluoride syringe filters. A 400 µL aliquot of the filtered extract was dried using a speed vacuum concentrator and stored at –80°C until analysis.

Prior to GC–MS analysis, the dried metabolites were chemically derivatized under a nitrogen atmosphere using N,O-bis(trimethylsilyl)trifluoroacetamide to improve their volatility and thermal stability. Chromatographic separation was performed on a fused silica capillary column coated with 5% diphenyl/95% dimethylpolysiloxane (20 m × 0.18 mm ID, 0.18 µm film thickness), with helium used as the carrier gas. The oven temperature was programmed to increase from 60°C to 340°C, over a 17.5-min period.

Each sample was spiked with nine internal standards (250 ng each) for

normalization and quality control: amylbenzene, 1-phenylhexane, 1-phenyloctane, 1-phenyldecane, 1-phenyldodecane, hexadecylbenzene, octadecylbenzene, tetradecylbenzene, and 2,6-di-tert-butyl-4-methylphenol. Mass spectrometric detection was conducted using a Thermo-Finnigan Trace DSQ fast-scanning single-quadrupole system equipped with electron impact (EI) ionization and operated in full-scan mode over a mass range of 50–750 m/z. Metabolites were annotated by comparing EI mass spectra and retention information against the NIST mass spectral library.

2.8 Metabolite Functional analysis

To evaluate the biological significance of the metabolomic alterations, pathway enrichment analysis was performed using MetaboAnalyst 6.0 (25). A list of annotated metabolites obtained from the GC-MS profiling was uploaded to the Enrichment Analysis module, and the compounds were mapped to KEGG identifiers using the default metabolite mapping function. Ambiguous or unmatched entries were excluded from analysis.

Overrepresentation analysis was performed using the KEGG metabolic pathway library as a reference. Statistical significance was assessed using a hypergeometric test, and pathways were ranked according to their enrichment ratios and corresponding nominal *P*-values. For visualization, the top 25 enriched metabolic pathways were selected and summarized in a bubble plot, in which the x-axis indicates $-\log_{10}$(P-value), bubble size represents the enrichment ratio, and bubble color reflects the degree of significance.

2.9 Multi-omics integration analysis

Microbiome and metabolomics data were integrated using Model-based Integration of Metabolite Observations and Species Abundances 2 (MIMOSA2; http://elbo–spice.cs.tau.ac.il/shiny/MIMOSA2shiny/). This framework enables the quantification of community-level metabolic potential (CMP) scores by modeling metabolite turnover within microbial communities based on species-level metabolic capabilities annotated in the KEGG database. MIMOSA2 supports paired microbiome–metabolome datasets and facilitates mechanistic interpretations by estimating the contribution of each taxon to metabolite production or consumption (26). The resulting scatterplots include trend lines indicating that the directionality of metabolite concentration changes with positive slopes for increases and negative slopes for decreases, along with corresponding R^2 values that represent the degree of association between CMP and metabolite levels. Contribution bar charts illustrate the proportional impact of individual taxa on metabolite variance, with positive and negative values indicating their potential roles in metabolite accumulation and depletion, respectively ($P < 0.1$).

To further explore host–microbiome metabolic interactions, a joint pathway analysis was performed using MetaboAnalyst 6.0 (25). This analysis integrated the DEG-abundant metabolites identified by MIMOSA2 with the host DEGs to uncover convergently modulated metabolic pathways. Pathway impact scores were computed to evaluate the relative significance of each pathway within the network, considering the pathway topology and metabolite–gene associations.

3. Results

3.1. *Transcriptomic profiling and differential gene expression analysis*

RNA sequencing of the ileal tissue generated 233,587,372 raw reads with an average GC content of 44.75%. After quality trimming, 230,054,530 clean reads were retained, exhibiting a slightly reduced GC content (44.58%). Alignment to the reference Sus scrofa genome resulted in an overall alignment rate of 84.8%, with 74.19% of the reads uniquely mapped (Table 1).

Differential expression analysis between the control and *L. plantarum* treatment groups identified 1,229 DEGs, including 662 upregulated and 567 downregulated transcripts, based on a threshold of $|\log_2 FC| \geq 1$ and FDR < 0.05 (Fig. 1).

3.2. *Functional enrichment analysis of DEGs*

Functional enrichment analysis of the DEGs in the ileum was performed using the DAVID database. Gene Ontology analysis revealed significant enrichment in immune-related biological processes, including the positive regulation of interleukin-6 production and actin filament organization, indicating the potential activation of immune responses and epithelial remodeling (Fig. 2).

In the cellular component category, DEGs were associated with structures such as phagocytic vesicles, Z discs, apical plasma membranes, and focal adhesions, implying alterations in membrane dynamics and epithelial barrier organization (Fig. 2).

KEGG pathway analysis identified multiple enriched pathways related to immune regulation and barrier function, such as the B-cell receptor signaling pathway,

nuclear factor kappa-light-chain-enhancer of activated B cells (NF-κB) signaling pathway, the intestinal immune network for IgA production, and leukocyte transendothelial migration. In addition, enrichment of tight junctions, mineral absorption, fat digestion and absorption, and general metabolic pathways suggests coordinated regulation of mucosal defense and nutrient absorption (Fig. 2).

To explore metabolic alterations induced by *L. plantarum* supplementation, untargeted metabolomic profiling of fecal samples was performed. Enrichment analysis using MetaboAnalyst6.0 revealed that DEG-abundant metabolites were predominantly associated with amino acid and lipid metabolism pathways (Fig. 3).

Specifically, valine, leucine, and isoleucine biosynthesis; glutathione metabolism; arginine and proline metabolism; and glycine, serine, and threonine metabolism were among the most enriched pathways. These pathways are closely linked to cellular repair, the oxidative stress response, and mucosal homeostasis.

Furthermore, the enrichment of linoleic acid metabolism, pantothenate and CoA biosynthesis, and butanoate metabolism suggests the potential modulation of fatty acid processing and short-chain fatty acid production. Notably, sphingolipid metabolism, although less prominently enriched, was also observed, implying its potential role in epithelial barrier dynamics.

Overall, metabolite-based pathway analysis indicates that *L. plantarum* supplementation alters key metabolic pathways in the gut environment, particularly those involved in nutrient absorption, redox balance, and epithelial support.

3.3. Fecal microbiome shifts post *L. plantarum* treatment

Alpha diversity analysis revealed that dietary supplementation with *L. plantarum* led to increased microbial richness and diversity in fecal samples, as evidenced by higher ACE, Chao1, Shannon, and Simpson indices than those in the control group (Fig. 4). These results suggest that *L. plantarum* intake enhances the ecological complexity of the gut microbiota in weaned piglets. This observation is consistent with previous studies reporting that dietary *L. plantarum* administration increases alpha diversity in the gastrointestinal microbiota, thereby contributing to improved gut microbial stability and resilience (5).

Taxonomic analysis at the genus level revealed compositional differences between the control and treatment groups (Fig. 5). Notably, the relative abundance of *Lactobacillus* increased in the plantarum-supplemented group, indicating the successful colonization or promotion of commensal lactic acid bacteria. In contrast, potentially pathogenic genera, such as *Shigella*, were markedly reduced, which may be attributed to competitive exclusion or pH-lowering effects associated with lactic acid production. Interestingly, an increase in the genus *Helicobacter* was observed in the treatment group. Although *Helicobacter* includes pathogenic species, its proliferation may reflect transient ecological shifts rather than pathogenic overgrowth.

3.4. Ileal Microbiota Functional Prediction

To investigate the functional implications of microbial compositional changes, predictive metagenomic analysis was performed based on 16S rRNA gene data (Fig. 6). Comparison of functional pathway abundance revealed significant enrichment of the NOD-like receptor signaling pathway in the *L. plantarum*-

supplemented group compared to that in the control group (P = 0.024). The NOD-like receptor family is integral to innate immune surveillance, recognizing intracellular microbial components and initiating downstream signaling cascades, including activation of NF-κB and inflammasome formation, ultimately leading to the production of proinflammatory cytokines and antimicrobial peptides.

3.5. Microbiota–Metabolite Associations Predicted by MIMOSA2

To elucidate the functional contributions of the gut microbiota to metabolite variation, an integrative analysis was performed using MIMOSA2, which infers CMP based on species abundance and genome-scale metabolic reconstructions. The analysis identified six metabolites that were significantly influenced by the microbiome composition: L-serine, nicotinate, L-proline, linoleate, pidolic acid, and D-phenylalanine (Fig. 7). For each metabolite, the CMP scores were calculated and matched to the metabolite abundance profiles, revealing taxa-specific associations (P < 0.1).

3.6. Integrated Metabolic Pathways Linking Ileal Transcriptome and Microbial Metabolites

To identify the functional convergence of host gene expression and microbial-derived metabolites, joint pathway analysis was conducted using MetaboAnalyst 6.0. Additionally, KEGG pathway integration was performed by combining the ileal DEGs with metabolites predicted using MIMOSA2. Nine metabolic pathways were identified as functional nodes between the host transcriptome and the microbial metabolome

based on both pathway impact and statistical enrichment (Fig. 8). Linoleic acid metabolism exhibited the greatest impact and significance. Glycerolipid metabolism, and cysteine and methionine metabolism also showed high statistical enrichment, whereas glycerophospholipid metabolism displayed a comparatively lower pathway impact but remained statistically significant.

3.7. Influence of microbiota–host interactions on host metabolic pathways

The alluvial diagram constructed from the integrated multi-omics analysis revealed extensive interactions between the ileal microbiota, microbially derived metabolites, host metabolic pathways, and host genes (Fig. 9). At the family level, the distinct microbial taxa were strongly associated with specific metabolites. *Helicobacteraceae* predominantly contributed to linoleate, L-proline, and L-serine metabolism, whereas *Enterobacteriaceae* were linked to linoleate, l-serine, and nicotinate metabolism. Additionally, *Prevotellaceae* was involved in the metabolism of L-proline, L-serine, and nicotinate; *Fusobacteriaceae* was primarily associated with nicotinate; and *Cerasicoccaceae* showed a specific relationship with pidolic acid. Integration of these microbial-derived metabolites with the host ileal transcriptome identified several metabolic pathways, notably linoleic acid metabolism; glycine, serine, and threonine metabolism; and sphingolipid metabolism as key nodes influenced by the microbiota during the weaning transition.

4. Discussion

A comprehensive multi-omics strategy was used to investigate the effects of dietary *L. plantarum* supplementation on host–microbiome interactions in weaned piglets. First, each omics layer was analyzed independently, including assessments of the ileal transcriptome, fecal microbiome, and fecal metabolome, to characterize the alterations induced by probiotic intake. The relationships between fecal microbiota and microbial-derived metabolites were examined to determine how specific taxa contributed to shifts in metabolite profiles. Metabolites that were significantly modulated by microbial activity were subsequently integrated with the ileal transcriptomic data to explore their associations with host gene expression. This integrative analysis provides a comprehensive understanding of how probiotic-induced changes in the gut microbial ecosystem and its metabolic outputs converge with host intestinal transcriptional responses during the postweaning transition.

4.1 Metabolic adaptation

Multi-omics integration revealed that *L. plantarum* supplementation strongly influenced host–microbiome metabolic interactions, particularly within the lipid and amino acid pathways. Linoleic acid metabolism exhibited the greatest impact (Fig. 8). Transcriptomic evidence showed increased *CYP1A2* expression, suggesting enhanced conversion of linoleic acid into epoxy-linoleates. Unlike other linoleic acid derivatives that can promote inflammatory signaling, epoxy-linoleates exert anti-inflammatory and cytoprotective effects, including the suppression of reactive oxygen species and preservation of tight junction protein expression (27-29). These effects are particularly

435 relevant during the postweaning transition, when piglets face high oxidative stress and
436 a heightened risk of barrier disruption.

437 Alterations in glycine, serine, and threonine metabolism were also evident.
438 Although *Helicobacteraceae* members were associated with serine consumption, host
439 transcriptional responses appeared to compensate through enhanced serine
440 biosynthesis. Specifically, the upregulation of *PHGDH* and *PGAM1* diverted
441 glycolytic intermediates toward serine production, whereas the downregulation of
442 *SDSL* limited the conversion of serine to glycine. This coordinated adjustment
443 promotes serine accumulation, which is critical for mucin production and membrane
444 phospholipid synthesis, thereby reinforcing epithelial protection (30-32).

445 Sphingolipid metabolism further suggested probiotic-driven remodeling.
446 Transcriptomic profiles showed reduced *SPHK2* expression, along with increased
447 *B4GALT6* expression, suggesting a shift toward ceramide retention and complex
448 glycosphingolipid synthesis (Fig. 9). These molecules are known to cluster within lipid
449 rafts, disperse pathogen receptors, and reduce microbial adherence (33, 34). Such
450 modulation suggests that *L. plantarum* supplementation may support both metabolic
451 stability and structural defense against pathogenic invasion.

452 Collectively, these findings highlight a coordinated metabolic adaptation in
453 which *L. plantarum* supplementation directs lipid and amino acid metabolism toward
454 pathways that reduce oxidative stress, stabilize tight junctions, and enhance mucosal
455 defense. These adjustments are likely central to maintaining intestinal integrity during
456 physiologically stressful weaning periods.

457

458 **4.2 Immune modulation**

In addition to metabolic adaptations, *L. plantarum* supplementation modulated immune-related processes at both the transcriptomic and microbiome levels. Gene Ontology and KEGG analyses revealed enrichment of pathways associated with interleukin-6 signaling, NF-κB activation, B cell receptor signaling, and IgA production, indicating that probiotic intake promoted immune responsiveness at multiple levels (Fig. 2). Collectively, these pathways contribute to mucosal defense by coordinating cytokine release, immune cell recruitment, and antibody production. Importantly, such effects are highly relevant in weaned piglets, whose adaptive immune systems remain immature; antigen-specific IgA responses typically become functional only after approximately six weeks of age (35). Therefore, the activation of immune pathways in response to *L. plantarum* may represent a compensatory mechanism that reinforces mucosal defense during this immunologically vulnerable period. However, these immune-related changes should be interpreted with caution because the piglets were not experimentally challenged with specific pathogens. Therefore, the observed immune responses may reflect enhanced mucosal preparedness rather than a pathogen-induced inflammatory response.

Microbiome analysis confirmed these immune-related changes. Alpha diversity indices, including ACE, Chao1, Shannon, and Simpson indices, were consistently higher in the *L. plantarum* group, reflecting a more balanced microbial ecosystem (Fig. 4). Enhanced microbial diversity is widely associated with greater functional redundancy and ecological resilience, allowing the gut microbiota to resist perturbations and outcompete opportunistic pathogens (36, 37). Taxonomic shifts supported this protective role; the abundance of *Lactobacillus* increased, while that of potentially pathogenic genera such as *Shigella* were reduced, consistent with probiotic-

mediated pathogen suppression via competitive exclusion and lactic acid production (2, 6) (Fig. 5).

Interestingly, a transient increase in *Helicobacter* was observed. This transient shift may also be associated with changes in gut pH, as lactic acid produced by probiotics can contribute to acidification, potentially influencing the relative abundance of acid-tolerant taxa such as *Helicobacter*. Although certain species within this genus can be pathogenic, previous studies have shown that acid-tolerant *Helicobacter* strains may expand temporarily when microbial competition decreases after weaning (37). This transient shift likely represents an ecological adjustment rather than harmful colonization, further underscoring the dynamic interplay between microbial competition and the host environment during the weaning transition.

Predictive metagenomic analysis provided additional evidence of immune modulation, revealing the enrichment of the NOD-like receptor signaling pathway in the *L. plantarum*-supplemented group (Fig. 6). NOD-like receptors act as critical intracellular sensors that detect microbial motifs and initiate downstream activation of NF-κB and inflammasome pathways, culminating in the production of cytokines and antimicrobial peptides (1). This suggests that probiotic supplementation may enhance innate immune preparedness, effectively bridging the gap until the adaptive immune system becomes fully functional.

Taken together, these findings demonstrate that *L. plantarum* supplementation not only reshapes the gut microbiota composition, but also strengthens mucosal immunity by stimulating innate defense pathways and promoting ecological stability. Such changes likely contribute to the reduced susceptibility to postweaning diarrhea and improved intestinal resilience.

4.3 Integrated host–microbiome interactions

The multi-omics framework used in this study revealed how *L. plantarum* supplementation shapes host–microbiome interactions during the postweaning transition. MIMOSA2 analysis identified taxon-specific contributions to metabolite turnover, with *Helicobacteraceae* linked to L-serine and L-proline consumption, *Prevotellaceae* and *Enterobacteriaceae* influencing both amino acid and nicotinate metabolism, and *Cerasicoccaceae* associated with pidolic acid production (Fig. 7). Conversely, metabolites such as linoleate, pidolic acid, and D-phenylalanine were predicted to be produced microbially, indicating that distinct bacterial taxa contributed to either consumption or production depending on the metabolic context. These findings highlight the division of metabolic labor within the gut microbiota and illustrate how probiotic-driven shifts reconfigure the luminal metabolite pool.

When host transcriptional responses were overlaid with microbial metabolite profiles, several convergent pathways emerged, including linoleic acid, glycerolipid, cysteine, methionine, and glycerophospholipid metabolism (Fig. 8). These pathways were closely associated with epithelial lipid remodeling, antioxidant defense, and cell membrane turnover, suggesting that probiotic supplementation fosters a metabolic environment conducive to epithelial resilience. Key host genes were identified as central mediators within these processes. *CYP1A2* directs linoleic acid toward epoxy-linoleates, reducing oxidative stress and reinforcing tight junctions. *PGAM1* and *PHGDH* enhanced serine biosynthesis, whereas *SDSL* downregulation limited serine catabolism, collectively ensuring serine retention for mucin and phospholipid synthesis. *B4GALT6* promotes glycosphingolipid formation that disperses pathogen receptors

within lipid rafts, thereby decreasing the opportunities for microbial adhesion.

Importantly, these host–microbiome adjustments did not operate in isolation but formed a coordinated network of interactions. While Sankey plot visualization reflects correlation rather than direct causation, the associations highlight functionally meaningful links (Fig. 9). For example, even though *Helicobacteraceae* transiently expanded and correlated with the consumption of L-serine and L-proline, host transcriptional adjustments compensated for the enhanced serine biosynthesis and restricted catabolism. This ensures sufficient serine availability for barrier-supportive functions, thereby maintaining the epithelial integrity in an environment with increased microbial competition. Probiotic supplementation buffers the potential negative effects of transient microbial shifts, with host metabolic compensation and enhanced microbial diversity, thereby preventing long-term destabilization.

Overall, these integrative findings illustrate that *L. plantarum* supplementation orchestrates a multilayered adaptation in which microbial taxa, metabolite profiles, and host gene expression converge to stabilize the intestinal barrier and promote immune preparedness. This systems-level interplay highlights the value of multi-omics approaches in uncovering mechanisms that would remain hidden under single-omics frameworks, providing a holistic understanding of how probiotics mitigate weaning-associated stress in piglets.

5. Conclusion

This study characterized the effects of *Lactobacillus plantarum* supplementation on host–microbiome interactions in weaned piglets using an integrated multi-omics approach. Probiotic supplementation increased microbial diversity, promoted beneficial bacterial populations, reduced potentially pathogenic taxa, and was associated with host transcriptional changes related to immune function, epithelial barrier maintenance, and metabolic regulation. Integrated analysis identified linoleic acid, glycine/serine/threonine, and sphingolipid metabolism as key pathways linking microbial and host responses. These findings indicate that *L. plantarum* may help improve intestinal resilience during weaning and provide mechanistic insight into its beneficial role in gut health. Practically, the microbial, metabolic, and host transcriptional signatures identified here may guide the development of targeted probiotic-based feed additives aimed at improving antioxidant capacity, mucosal immune preparedness, and metabolic stability during the postweaning period. Such strategies may help reduce weaning-associated intestinal stress and support healthier growth in commercial swine production.

Acknowledgments

This work was supported by Korea Institute of Planning and Evaluation for Technology in Food, Agriculture and Forestry(IPET) through Agricultural Microbiome R&D Program for Advancing innovative technology Program(or Project), funded by Ministry of Agriculture, Food and Rural Affairs(MAFRA)(RS-2025-02216704) and was supported by the Chung-Ang University Research Grants in 2024.

References

1. Tang X, Xiong K, Fang R, Li M. Weaning stress and intestinal health of piglets: A review. Front Immunol. 2022;13:1042778.

2. Hu T, Song ZG, Yang L, Chen KY, Wu Y, Xie F, et al. Maternal probiotic mixture supplementation optimizes the gut microbiota structure of offspring piglets through the gut-breast axis. Animal Nutrition. 2024;19:386-400.

3. Tang Q, Lan T, Zhou C, Gao J, Wu L, Wei H, et al. Nutrition strategies to control post-weaning diarrhea of piglets: From the perspective of feeds. Anim Nutr. 2024;17:297-311.

4. Liao SF, Nyachoti M. Using probiotics to improve swine gut health and nutrient utilization. Anim Nutr. 2017;3(4):331-43.

5. Wang TW, Teng KL, Liu YY, Shi WX, Zhang J, Dong EQ, et al. PFM 105 Promotes Intestinal Development Through Modulation of Gut Microbiota in Weaning Piglets. Frontiers in Microbiology. 2019;10:90.

6. Wang J, Zeng Y, Wang S, Liu H, Zhang D, Zhang W, et al. Swine-Derived Probiotic Lactobacillus plantarum Inhibits Growth and Adhesion of Enterotoxigenic Escherichia coli and Mediates Host Defense. Front Microbiol. 2018;9:1364.

7. Lourenco JM, Hampton RS, Johnson HM, Callaway TR, Rothrock MJ, Jr., Azain MJ. The Effects of Feeding Antibiotic on the Intestinal Microbiota of Weanling Pigs. Front Vet Sci. 2021;8:601394.

8. Manyi-Loh C, Mamphweli S, Meyer E, Okoh A. Antibiotic Use in Agriculture and Its Consequential Resistance in Environmental Sources: Potential Public Health Implications. Molecules. 2018;23(4):795.

9. Yu J, Zuo B, Li Q, Zhao F, Wang J, Huang W, et al. Dietary supplementation with Lactiplantibacillus plantarum P-8 improves the growth performance and gut microbiota of weaned piglets. Microbiology spectrum. 2024;12(2):e02345-22.

10. Kobayashi N, Takahashi D, Takano S, Kimura S, Hase K. The Roles of Peyer's Patches and Microfold Cells in the Gut Immune System: Relevance to Autoimmune Diseases. Front Immunol. 2019;10:2345.

11. Callahan BJ, McMurdie PJ, Rosen MJ, Han AW, Johnson AJ, Holmes SP. DADA2: High-resolution sample inference from Illumina amplicon data. Nat Methods. 2016;13(7):581-3.

12. Simms D, Cizdziel PE, Chomczynski P. TRIzol: A new reagent for optimal single-step isolation of RNA. Focus. 1993;15(4):532-5.

13. Andrews S. FastQC: A quality control tool for high throughput sequence data Cambridge, United Kingdom: Babraham Bioinformatics; 2010 [Available from: https://www.bioinformatics.babraham.ac.uk/projects/fastqc/].

14. Bolger AM, Lohse M, Usadel B. Trimmomatic: a flexible trimmer for Illumina sequence data. Bioinformatics. 2014;30(15):2114-20.

15. Kim D, Langmead B, Salzberg SL. HISAT: a fast spliced aligner with low memory requirements. Nat Methods. 2015;12(4):357-60.

16. Li H, Handsaker B, Wysoker A, Fennell T, Ruan J, Homer N, et al. The Sequence Alignment/Map format and SAMtools. Bioinformatics. 2009;25(16):2078-9.

17. Liao Y, Smyth GK, Shi W. featureCounts: an efficient general purpose program for assigning sequence reads to genomic features. Bioinformatics. 2014;30(7):923-30.

18. Robinson MD, Oshlack A. A scaling normalization method for differential expression analysis of RNA-seq data. Genome Biol. 2010;11(3):R25.

621 19. Ritchie ME, Phipson B, Wu D, Hu Y, Law CW, Shi W, et al. limma powers
622 differential expression analyses for RNA-sequencing and microarray studies. Nucleic
623 Acids Res. 2015;43(7):e47.
624 20. Wickham H. Programming with ggplot2. Ggplot2: elegant graphics for data
625 analysis: Springer; 2016. p. 241-53.
626 21. Ashburner M, Ball CA, Blake JA, Botstein D, Butler H, Cherry JM, et al. Gene
627 ontology: tool for the unification of biology. The Gene Ontology Consortium. Nat
628 Genet. 2000;25(1):25-9.
629 22. Kanehisa M, Goto S. KEGG: kyoto encyclopedia of genes and genomes. Nucleic
630 Acids Res. 2000;28(1):27-30.
631 23. Sherman BT, Hao M, Qiu J, Jiao X, Baseler MW, Lane HC, et al. DAVID: a web
632 server for functional enrichment analysis and functional annotation of gene lists (2021
633 update). Nucleic Acids Res. 2022;50(W1):W216-W21.
634 24. Supek F, Bosnjak M, Skunca N, Smuc T. REVIGO summarizes and visualizes
635 long lists of gene ontology terms. PLoS One. 2011;6(7):e21800.
636 25. Pang Z, Lu Y, Zhou G, Hui F, Xu L, Viau C, et al. MetaboAnalyst 6.0: towards a
637 unified platform for metabolomics data processing, analysis and interpretation. Nucleic
638 Acids Res. 2024;52(W1):W398-W406.
639 26. Noecker C, Eng A, Muller E, Borenstein E. MIMOSA2: a metabolic network-
640 based tool for inferring mechanism-supported relationships in microbiome-
641 metabolome data. Bioinformatics. 2022;38(6):1615-23.
642 27. Rao R. Oxidative stress-induced disruption of epithelial and endothelial tight
643 junctions. Front Biosci. 2008;13:7210-26.
644 28. Yamagata K, Tagami M, Takenaga F, Yamori Y, Nara Y, Itoh S. Polyunsaturated

645 fatty acids induce tight junctions to form in brain capillary endothelial cells.
646 Neuroscience. 2003;116(3):649-56.
647 29. Lu J, Shang X, Zhong W, Xu Y, Shi R, Wang X. New insights of CYP1A in
648 endogenous metabolism: a focus on single nucleotide polymorphisms and diseases.
649 Acta Pharm Sin B. 2020;10(1):91-104.
650 30. Klomp LW, de Koning TJ, Malingre HE, van Beurden EA, Brink M, Opdam FL,
651 et al. Molecular characterization of 3-phosphoglycerate dehydrogenase deficiency--a
652 neurometabolic disorder associated with reduced L-serine biosynthesis. Am J Hum
653 Genet. 2000;67(6):1389-99.
654 31. Katane M, Nakasako K, Yako K, Saitoh Y, Sekine M, Homma H. Identification
655 of an l-serine/l-threonine dehydratase with glutamate racemase activity in mammals.
656 Biochem J. 2020;477(21):4221-41.
657 32. He L, Ding Y, Zhou X, Li T, Yin Y. Serine signaling governs metabolic
658 homeostasis and health. Trends Endocrinol Metab. 2023;34(6):361-72.
659 33. Tokuda N, Numata S, Li XJ, Nomura T, Takizawa M, Kondo Y, et al. β4GalT6 is
660 involved in the synthesis of lactosylceramide with less intensity than β4GalT5.
661 Glycobiology. 2013;23(10):1175-83.
662 34. Nakayama H, Iwabuchi K. Glycosphingolipid-Enriched Lipid Rafts-Mediated
663 Pathogen Recognition Systems. Trends in Glycoscience and Glycotechnology.
664 2019;31(184):E141-E9.
665 35. Stokes CR. The development and role of microbial-host interactions in gut
666 mucosal immune development. J Anim Sci Biotechnol. 2017;8(1):12.
667 36. Shin D, Chang SY, Bogere P, Won K, Choi JY, Choi YJ, et al. Beneficial roles of
668 probiotics on the modulation of gut microbiota and immune response in pigs. PLoS

One. 2019;14(8):e0220843.

37. Karasova D, Crhanova M, Babak V, Jerabek M, Brzobohaty L, Matesova Z, et al. Development of piglet gut microbiota at the time of weaning influences development of postweaning diarrhea - A field study. Res Vet Sci. 2021;135:59-65.

Table 1. A summary of RNA-seq preprocessing data

No	Sample name	Treat	Tissue	Raw Data		After Trimmomatic		Trimming Rate	Mapping data	
				reads	%GC	reads	%GC	(%)	Uniquely mapped read (%)	Overall alignment rate (%)
1	PC2_1	Control	Ileum	20,193,852	46	20,159,089	46	0.17	72.49%	83.24%
2	PC2_2	Control	Ileum	20,193,852	47	19,606,972	46	2.91		
3	PC55_1	Control	Ileum	18,998,585	45	18,966,193	45	0.17	71.27%	82.39%
4	PC55_2	Control	Ileum	18,998,585	45	18,431,225	45	2.99		
5	PC168_1	Control	Ileum	19,337,119	45	19,304,289	44	0.17	75.96%	86.98%
6	PC168_2	Control	Ileum	19,337,119	46	18,714,497	44	3.22		
7	T475_1	Plantarum	Ileum	19,594,243	44	19,562,994	44	0.16	72.94%	83.53%
8	T475_2	Plantarum	Ileum	19,594,243	44	19,072,770	44	2.66		
9	T478_1	Plantarum	Ileum	20,664,445	44	20,633,310	43	0.15	76.59%	86.62%
10	T478_2	Plantarum	Ileum	20,664,445	44	20,105,695	45	2.70		
11	T4175_1	Plantarum	Ileum	18,005,442	43	17,978,103	45	0.15	75.90%	86.12%
12	T4175_2	Plantarum	Ileum	18,005,442	44	17,519,393	44	2.70		

Figure legends

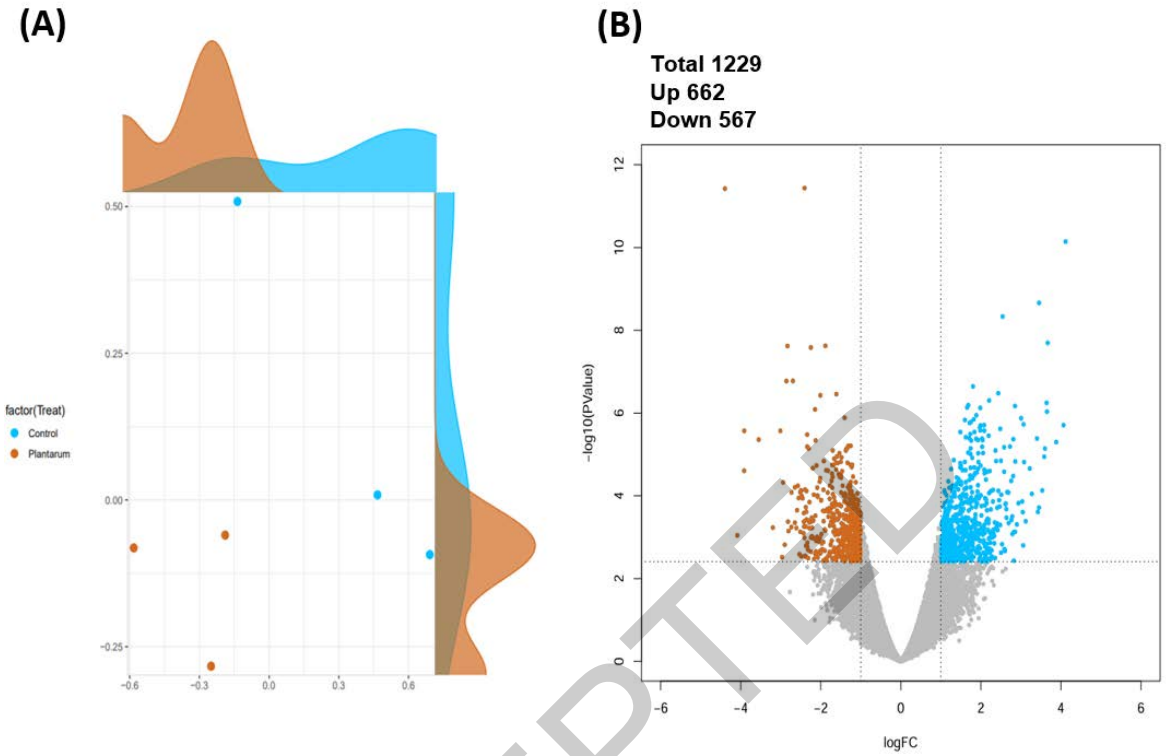

Figure 1. Transcriptional profiling in the weaned piglet ileum and functional differentially expressed gene (DEG**)** analysis.

(A) Multidimensional scaling; each point represents an individual sample. Blue and brown dots indicate control and plantarum groups. (B) DEGs volcano plot overview. log2FCs in Control-to-Plantarum gene expression ratios and $-\log_{10}$(P-value) are indicated on the x and y axes. Blue dots denote 662 significantly upregulated DEGs and brown dots denote 567 significantly down regulated DEGs (false discovery rate < 0.05), and vertical lines establish the two FC thresholds (absolute log2 FC ≥ 1). Key genes discussed in the manuscript (*CYP1A2*, *PHGDH*, *SPHK2*, and *B4GALT6*) are labeled.

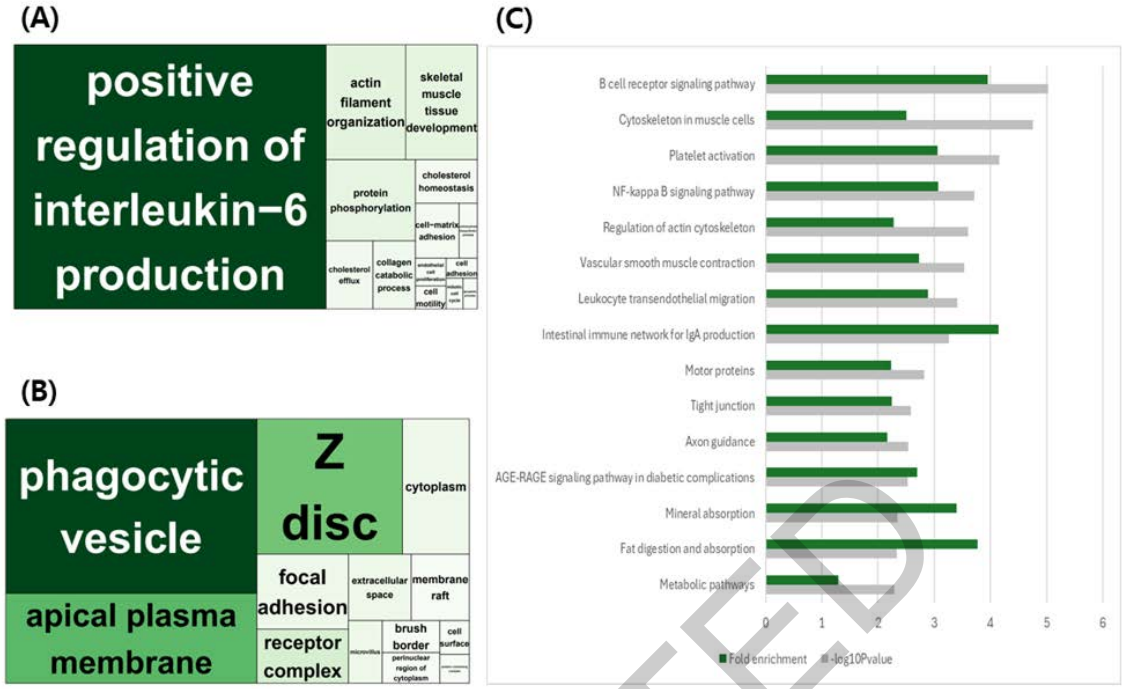

688

689 **Figure 2.** Gene Ontology (GO) tree map and Kyoto Encyclopedia of Genes and Genomes

690 (KEGG) pathways of Total differentially expressed gene (DEGs).

691 (A–B) Tree maps showing GO enrichment in ileal tissue. The size of each box

692 corresponds to the $-\log_{10}$(*P*-value) of the GO term, with larger boxes indicating more

693 significant enrichment. (A) Biological Process (BP); (B) Cellular Component. (C) KEGG

694 pathway analysis of all DEGs. The x-axis represents the fold enrichment and the $-\log_{10}$

695 (*P*-value), using the original *P*-values returned by the enrichment analysis.

696

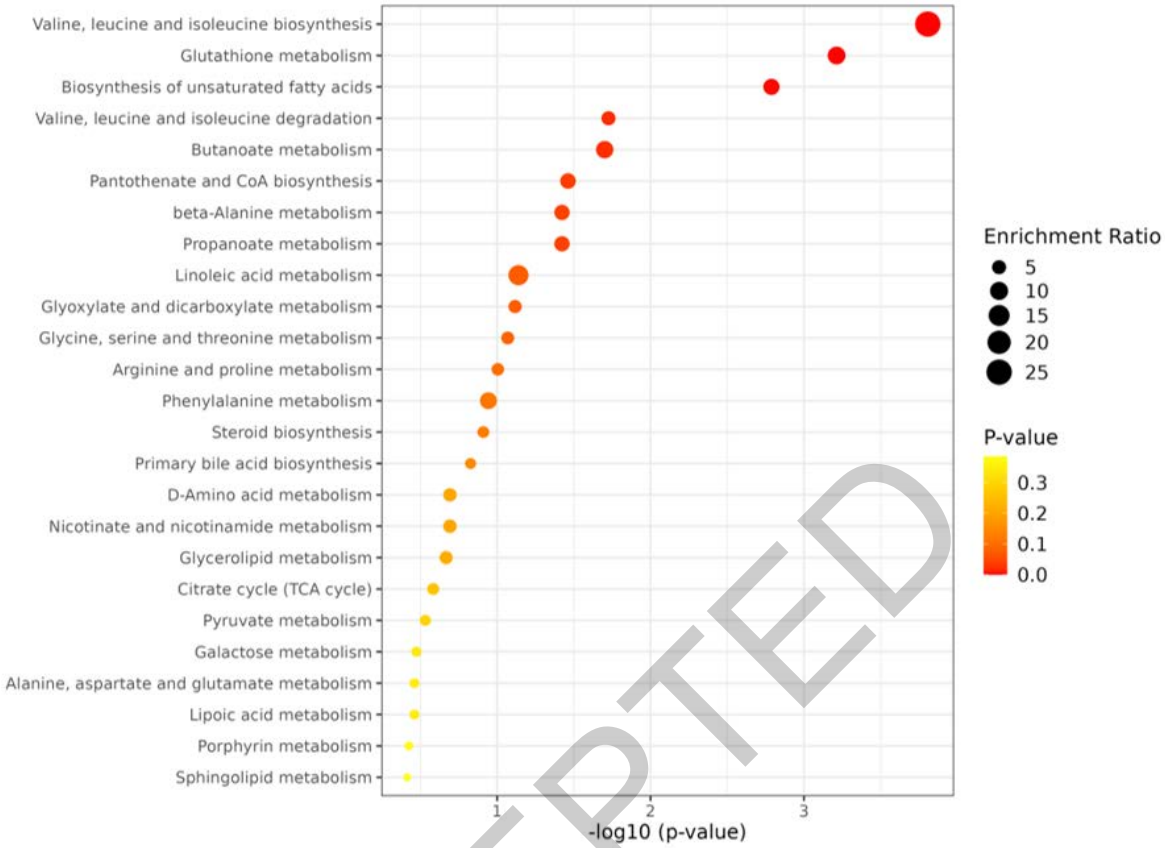

Figure 3. Overview of enriched metabolic pathways based on fecal metabolomic profiling.

Bubble plot showing the top 25 enriched metabolite sets identified using MetaboAnalyst 6.0. The x-axis represents the statistical significance of pathway enrichment ($-\log_{10}(P\text{-value})$, using the original P-values returned by the enrichment analysis), and the y-axis lists the associated metabolic pathways. The size of each circle indicates the enrichment ratio, while the color gradient from yellow to red reflects increasing statistical significance (i.e., lower *P*-values).

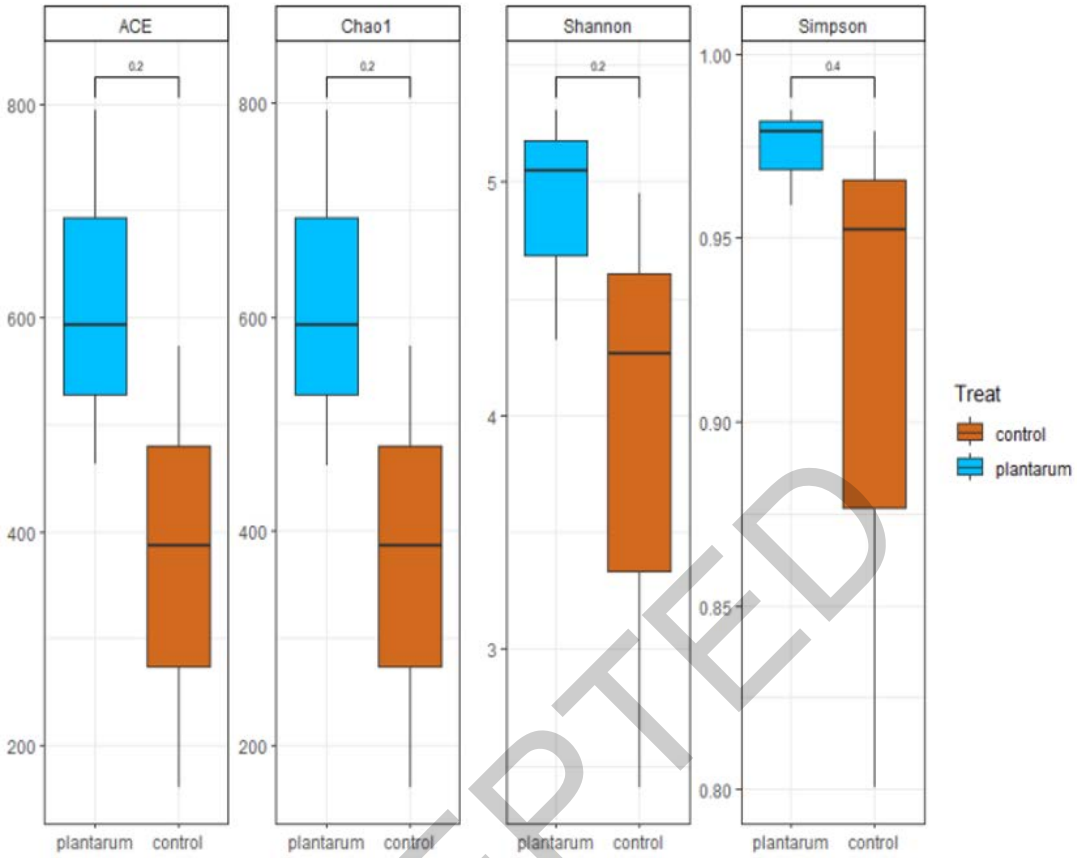

706

707 **Figure 4.** Comparison of alpha diversity indices between control and *Lactobacillus*

708 *plantarum*-treated piglets.

709 Box plots show microbial diversity metrics based on ACE, Chao1, Shannon, and

710 Simpson indices in fecal samples (n = 3 per group).

711

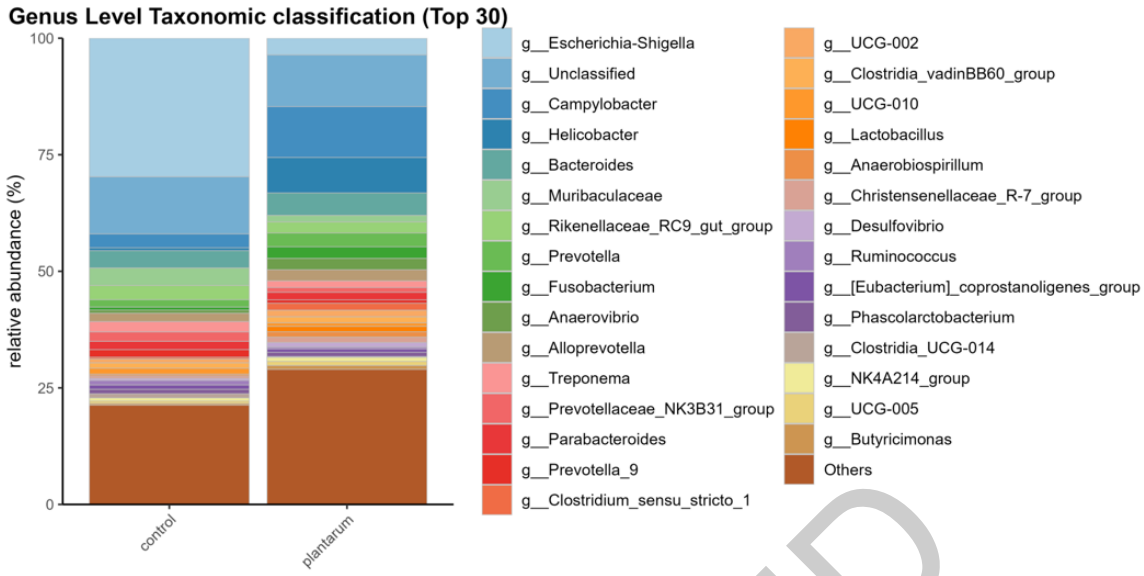

712

713 **Figure 5.** Genus-level composition of the fecal microbiota in control and *Lactobacillus*

714 *plantarum*-treated piglets.

715 The stacked bar chart illustrates the relative abundance (%) of bacterial genera identified

716 in fecal samples from the control (n = 3) and *L. plantarum*-supplemented (n = 3) groups.

717 Dominant taxa include *Escherichia-Shigella*, *Prevotella*, *Bacteroides*, and *Treponema*.

718 Notably, *Lactobacillus* and *Helicobacter* showed increased proportions in the *L.*

719 *plantarum* group, while *Escherichia-Shigella* was more prominent in the control group.

720 “Others” includes genera with low abundance (< 1%) or unclassified taxa.

721

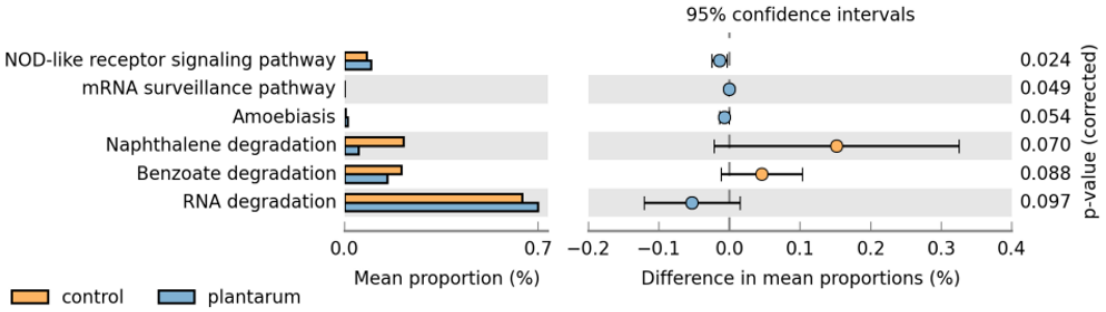

722

723 **Figure 6.** Functional analysis of fecal microbiota based on Kyoto Encyclopedia of Genes
724 and Genomes (KEGG) pathway predictions.

725 Statistically significant microbial pathways ($p < 0.1$), inferred from KEGG annotations,
726 are shown using statistical analysis of taxonomic and functional profiles generated bar
727 plots. Orange bars indicate pathways enriched in the Control group, while blue bars
728 indicate those enriched in the *Lactobacillus plantarum* treated group. The difference in
729 mean proportions reflects the predicted contribution difference of each pathway between
730 groups.

731

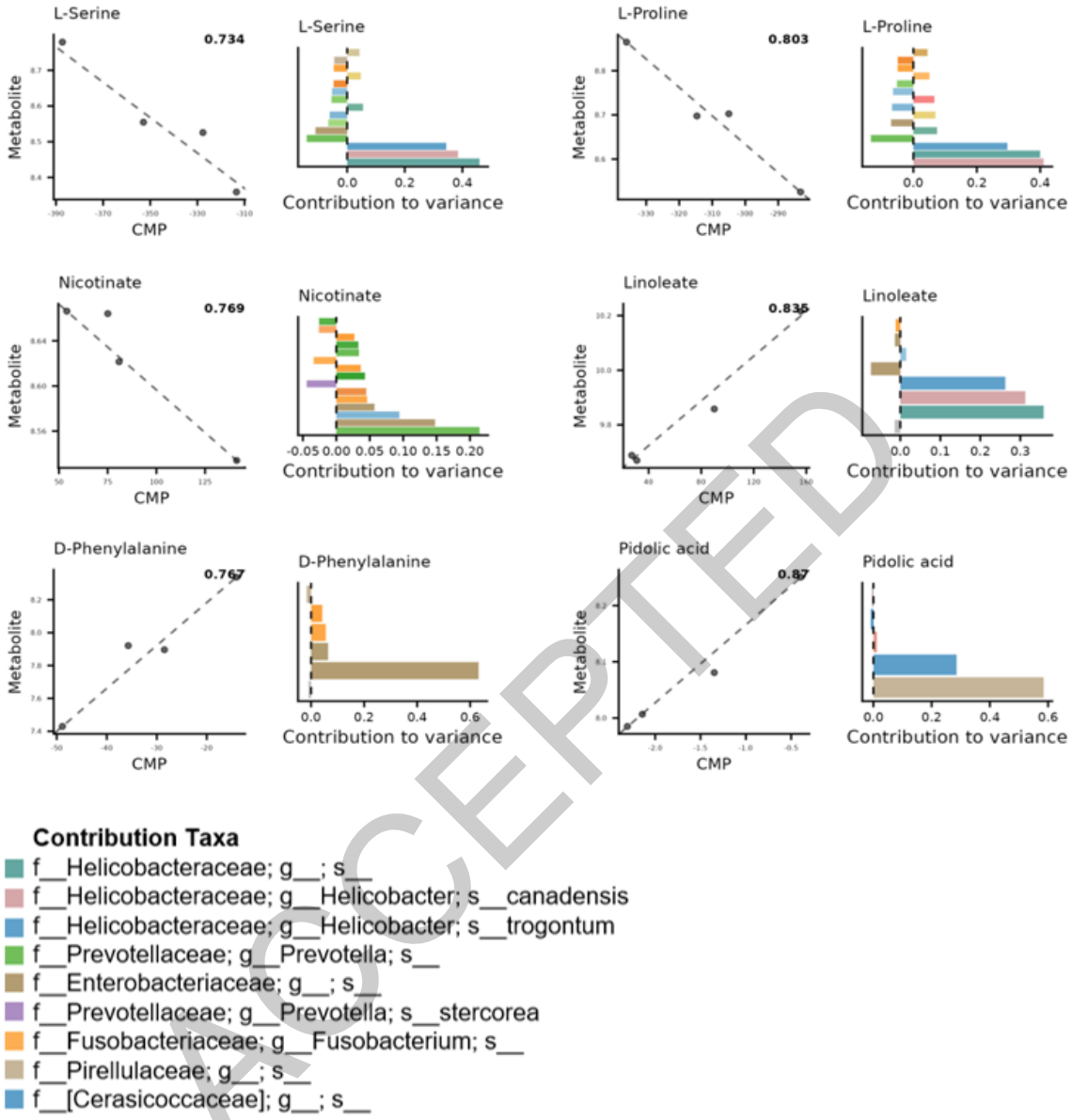

Figure 7. Integrative analysis of microbial taxa and associated fecal metabolites. The left panels display the relationship between metabolite concentrations and corresponding community metabolic potential (CMP) scores, with trend lines and R^2 values indicating the strength of the model fit. The right panels present the contribution of individual microbial taxa to the observed variance in metabolite levels. Bars extending to the right of the vertical axis represent taxa contributing to metabolite production, whereas those to

740 the left indicate taxa associated with metabolite consumption. Color-coded bars
741 correspond to specific bacterial taxa, as indicated in the legend.
742

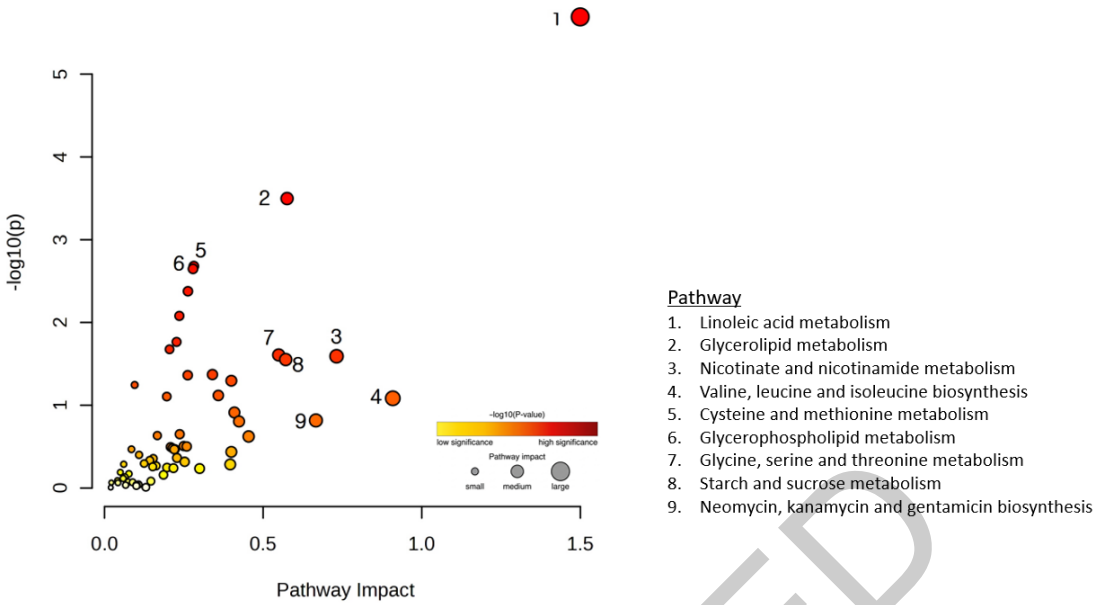

Figure 8. Integrated pathway analysis of ileal gene expression and microbial metabolite profiles.

This bubble plot illustrates the outcome of joint pathway analysis combining host transcriptomic and microbial metabolomic data using MetaboAnalyst 6.0 (https://www.metaboanalyst.ca/). The x-axis represents the pathway impact score calculated through topological analysis (degree centrality), and the y-axis corresponds to the statistical significance expressed as $-\log_{10}(P\text{-value})$, using the original *P*-values returned by the enrichment analysis. Each circle (node) represents a metabolic pathway, with its color indicating significance level (red = high significance, yellow = moderate significance, white = low significance) and its size reflecting the relative pathway impact. Enrichment analysis was conducted using the hypergeometric test, and integration was performed via the combined queries method. The eight most significantly enriched pathways are labeled, reflecting key overlaps between microbial metabolite changes and host transcriptional responses during the postweaning phase.

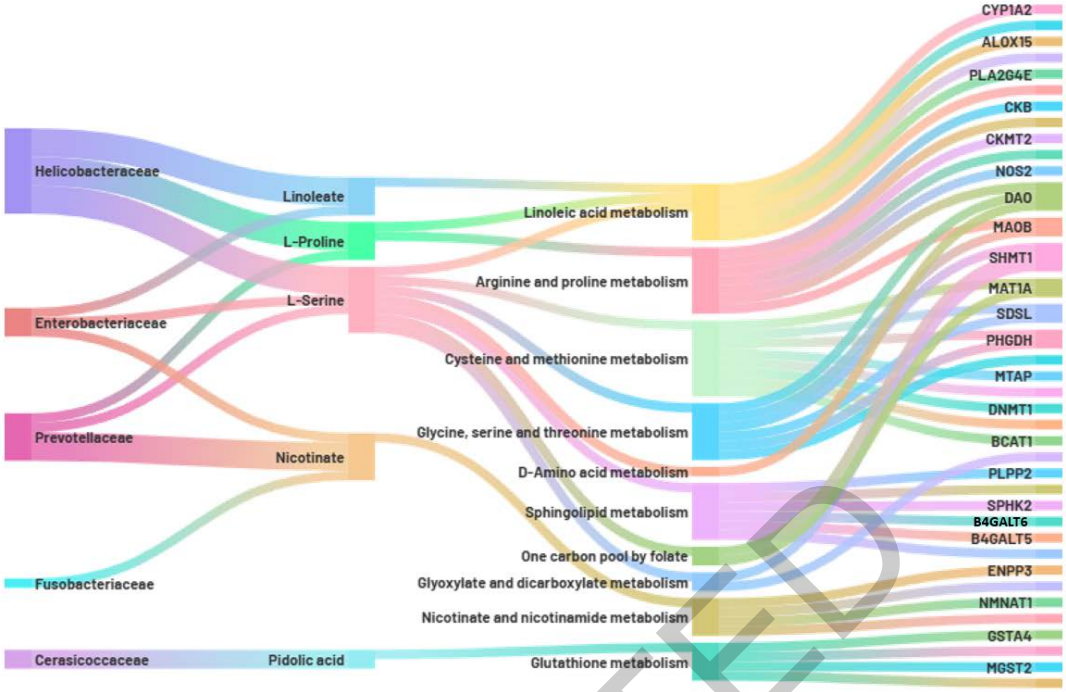

758

759 **Figure 9.** Integrated network of fecal microbiota, microbially derived metabolites, and
760 host gene expression during the weaning**.**

761 This figure provides an integrated overview of host–microbiome interactions during the
762 weaning period, illustrating the connections among fecal microbial taxa, microbially
763 derived metabolites, host metabolic pathways, and differentially expressed host genes.
764 Associations were identified through combined analysis using community metabolic
765 potential scores obtained from MIMOSA2, and pathway influence scores derived from
766 joint pathway analysis. The resulting network highlights putative functional linkages
767 between microbial activity and host gene regulation. Visualization was generated using
768 Flourish.